Journal of Alloys and Compounds 509 (2011) 4563–4568

Contents lists available at ScienceDirect

Journal of Alloys and Compounds

journal homepage: www.elsevier.com/locate/jallcom

Phase transition of Ni–Mn–Ga alloy powders prepared by vibration ball milling

B. Tian[a,b], F. Chen[a], Y.X. Tong[a], L. Li[a], Y.F. Zheng[a,c,*], Y. Liu[a,d], Q.Z. Li[b]

[a] Center for Biomedical Materials and Engineering, Harbin Engineering University, Harbin 150001, China
[b] Department of Chemical and Metallurgical Engineering, University of Nevada, Reno, NV 89557, USA
[c] Department of Advanced Materials and Nanotechnology, College of Engineering, Peking University, Beijing 100871, China
[d] School of Mechanical Engineering, The University of Western Australia, Crawley, WA 6009, Australia

ARTICLE INFO

Article history:
Received 5 October 2010
Received in revised form 17 January 2011
Accepted 18 January 2011
Available online 22 January 2011

Keywords:
Metals and alloys
Crystal structure
Shape memory
Phase transitions
X-ray diffraction

ABSTRACT

This study investigated the phase transformation of the flaky shaped Ni–Mn–Ga powder particles with thickness around 1 μm prepared by vibration ball milling and post-annealing. The SEM, XRD, DSC and ac magnetic susceptibility measurement techniques were used to characterize the Ni–Mn–Ga powders. The structural transition of Heusler → disordered fcc occurred in the powders prepared by vibration ball milling (high milling energy) for 4 h, which was different from the structural transition of Heusler → disordered fct of the powders fabricated by planetary ball milling (low milling energy) for 4 h. The two different structures after ball milling should be due to the larger lattice distortion occurred in the vibration ball milling process than in the planetary ball milling process. The structural transition of disordered fcc → disordered bcc took place at ~320 °C during heating the as-milled Ni–Mn–Ga powders, which was attributed to the elimination of lattice distortion caused by ball milling. The activation energy for this transition was 209 ± 8 kJ/mol. The Ni–Mn–Ga powder annealed at 800 °C mainly contained Heusler austenite phase at room temperature and showed a low volume of martensitic transformation upon cooling. The inhibition of martensitic transformation might be attributed to the reduction of grain size in the annealed Ni–Mn–Ga particles.

1. Introduction

Ni–Mn–Ga ferromagnetic shape memory alloys (FSMA) have drawn much attention in the past decades because of their large magnetic field induced strain (MFIS) and high response frequency [1–4]. Nevertheless, Ni–Mn–Ga alloys are very brittle, which remarkably impedes their practical applications. To overcome the problem, several forms based on the alloy have been proposed and investigated, including thin films [5–9], ribbons [10–12] and composites consisting of ductile polymer matrix and Ni–Mn–Ga alloy particles [13–20]. Among these forms, the composites prepared by mixing Ni–Mn–Ga alloy particles and polymer matrix exhibit great advantages with good formability and low cost of production, compared with the thin films and ribbons which are often restricted by their dimension in applications. In the Ni–Mn–Ga particle/polymer composites, Ni–Mn–Ga particles realizing the desired functions are critical for the performance of the composite.

Recently, spark erosion [21] has been used to prepare the Ni–Mn–Ga particles by rapidly solidifying the molten alloy droplets in liquid nitrogen or argon. Clearly, this is a complex and high cost process for preparing Ni–Mn–Ga particles. In comparison with spark erosion, ball milling is more simple and cost-effective in preparing the Ni–Mn–Ga particles due to the brittleness of the Ni–Mn–Ga alloy. Therefore, in our previous studies [22–24], ball milling method has been employed to fabricate Ni–Mn–Ga particles and the structural evolution of the particles has been preliminarily investigated. It was found that the $Ni_{49.8}Mn_{28.5}Ga_{21.7}$ micro-particles prepared by planetary ball milling show the disordered face centered tetragonal (fct) structure, whereas the particles prepared by vibration ball milling with similar milling parameters show a disordered face centered cubic (fcc) structure [24]. The effect of ball milling method on the structure of Ni–Mn–Ga particles has not been fully understood. Wang et al. [25] observed a structural transition from Heusler to disordered fcc structure in Ni_2MnGa nano-particles prepared by ball milling for 8 h using a SPEX-8000 laboratory miller, which is similar with our result obtained by vibration ball milling. They found that, after annealing at 350 °C, the Ni_2MnGa nano-particles could transform completely from austenite phase to martensite phase upon cooling. However, the martensitic transformation of the $Ni_{49.8}Mn_{28.5}Ga_{21.7}$ particles with disordered fcc structure has not been recovered even after annealing at 600 °C [24]. The above results indicate that the phase transition process of the Ni–Mn–Ga particles with disordered fcc structure is still unclear. In this study, the phase transition of the

* Corresponding author at: Department of Advanced Materials and Nanotechnology, College of Engineering, Peking University, Yi-He-Yuan Road, Hai-Dian District, Beijing 100871, China. Tel.: +86 10 6276 7411; fax: +86 10 6276 7411.
E-mail address: yfzheng@pku.edu.cn (Y.F. Zheng).

0925-8388/$ – see front matter © 2011 Elsevier B.V. All rights reserved.
doi:10.1016/j.jallcom.2011.01.104

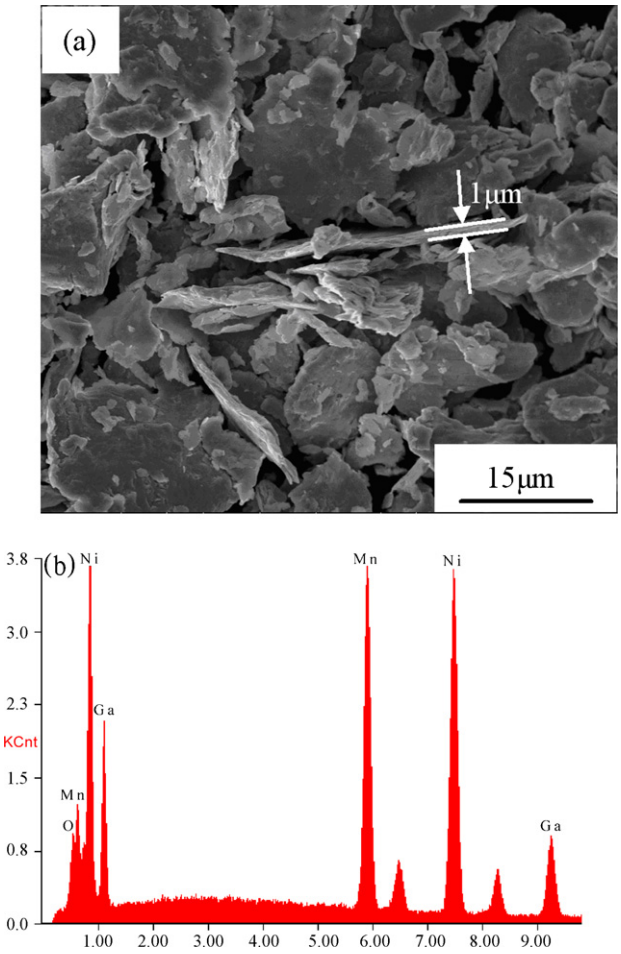

Fig. 1. (a) SEM image of as-milled Ni–Mn–Ga powders after 4 h milling and (b) EDS spectrum of this sample.

Ni–Mn–Ga particles after ball milling and post-annealing is further investigated and discussed.

2. Experimental details

A button-like polycrystalline $Ni_{49.8}Mn_{28.5}Ga_{21.7}$ alloy ingot was prepared by arc melting in argon atmosphere from high purity elements. The solidified ingot was homogenized at 850 °C for 10 h in vacuum followed by water-quenching, then crushed into particles with size ~3 mm and milled for 4 h in a QM-3A vibration ball mill (Nanjing University Instrument Plant, China) with hardened steel balls in a ball-to-powder weight ratio of 10:1. The milling speed was 1400 rpm. Acetone was added in the vial as the milling medium. To avoid overheating, cycles of 0.5 h milling and 1 h rest were performed. The as-milled powders were sealed in quartz tubes under high vacuum and annealed at different temperatures for 1 h.

The microstructure of the powders was observed using a FEI Quanta200 scanning electron microscope (SEM) equipped with energy dispersive spectrometry (EDS) analyzer. X-ray diffraction (XRD) analysis was carried out at room temperature using a Panalytical X-pert PRO diffractometer with Cu Kα radiation. A Perkin-Elmer Diamond differential scanning calorimeter (DSC) was used to investigate the annealing behavior and martensitic transformation. The temperature dependence of low-field ac magnetic susceptibility was also measured to determine the martensitic transformation and magnetic transition.

3. Results and discussion

Fig. 1 shows SEM micrograph and the EDS spectrum for the typical Ni–Mn–Ga powders milled for 4 h. It is seen that the particles with a size ranging from 1 to 15 μm are mostly flaky shape. The thickness of particles is ~1 μm, as indicated in Fig. 1(a). This is different from the result [22] in which the polygon shape powder particles are obtained by the planetary ball milling with similar milling parameters, which should result from the fact that the

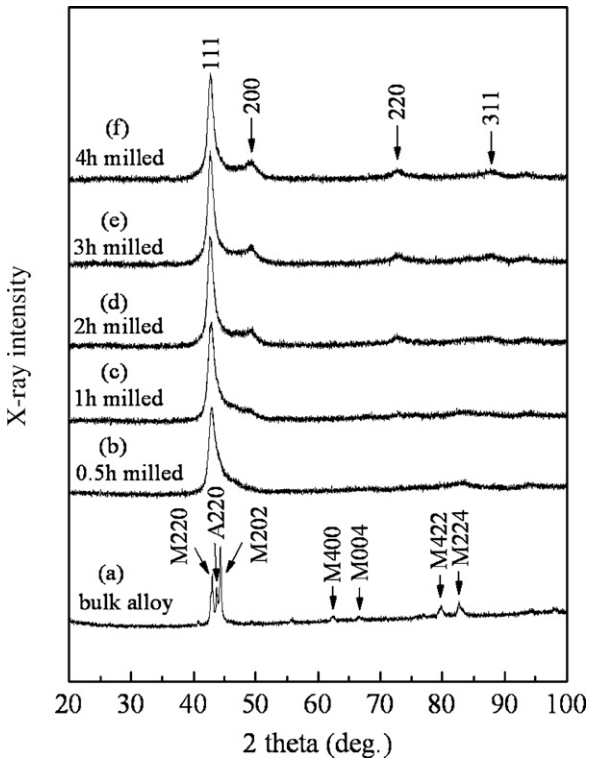

Fig. 2. Room temperature XRD patterns of Ni–Mn–Ga bulk alloy (a) and as-milled Ni–Mn–Ga powders after milling for 0.5 h (b), 1 h (c), 2 h (d), 3 h (e) and 4 h (f).

vibration ball mill provides more milling energy than the planetary ball mill to lead to a more severe deformation of the particles. Fig. 1(b) shows the EDS spectrum of the powders milled for 4 h, revealing a minor contamination of O, due to the slight oxidation of Mn on the surface of the Ni–Mn–Ga particles.

Fig. 2 shows the room temperature XRD patterns of the bulk Ni–Mn–Ga alloy and as-milled Ni–Mn–Ga powders. The original bulk Ni–Mn–Ga alloy is composed of a 5 M tetragonal martensite phase and Heusler austenite phase [22,23], as shown in Fig. 2(a). The lattice parameter of the austenite is $a = 0.58388$ nm and the lattice parameters of the tetragonal martensite are $a = 0.5948$ nm and $c = 0.5600$ nm. Fig. 2(b)–(f) shows the results of Ni–Mn–Ga powders milled for different times. After 0.5 h milling, the diffraction peaks corresponding to the martensite and austenite phases disappeared and a new diffraction peak centered at $2\theta = 42.7°$ appeared. With milling time increasing up to 4 h, the other three diffraction peaks centered at $2\theta = 49.6°$, 73.0° and 88.4° gradually became visible. These new diffraction peaks can be indexed as a disordered fcc structure with a lattice parameter of $a = 0.36646$ nm, which is similar to the result reported by Wang et al. [25].

Different from the disordered fcc structure obtained in the present ball milling process, a disordered fct structure was observed in the Ni–Mn–Ga powders prepared by planetary ball milling, the lattice parameters of the fct structure phase are $a = 0.39060$ nm and $c = 0.65479$ nm [22]. A schematic illustration for the structural transition from Heusler structure to disordered fct and disordered fcc is shown in Fig. 3. In the ball milling process, the mutual collision among the balls, vial wall and the alloy particles occurs. The lattice distortion, vacancy and other defects are introduced to the Ni–Mn–Ga alloy and the atomic order of the Ni–Mn–Ga alloy is destroyed during the process.

For the process with low milling energy (planetary ball milling), the fct structure as circled by black line in the upper part of Fig. 3 is assumed to occur in the disordered structure. For comparison with fct structure, the lattice constants

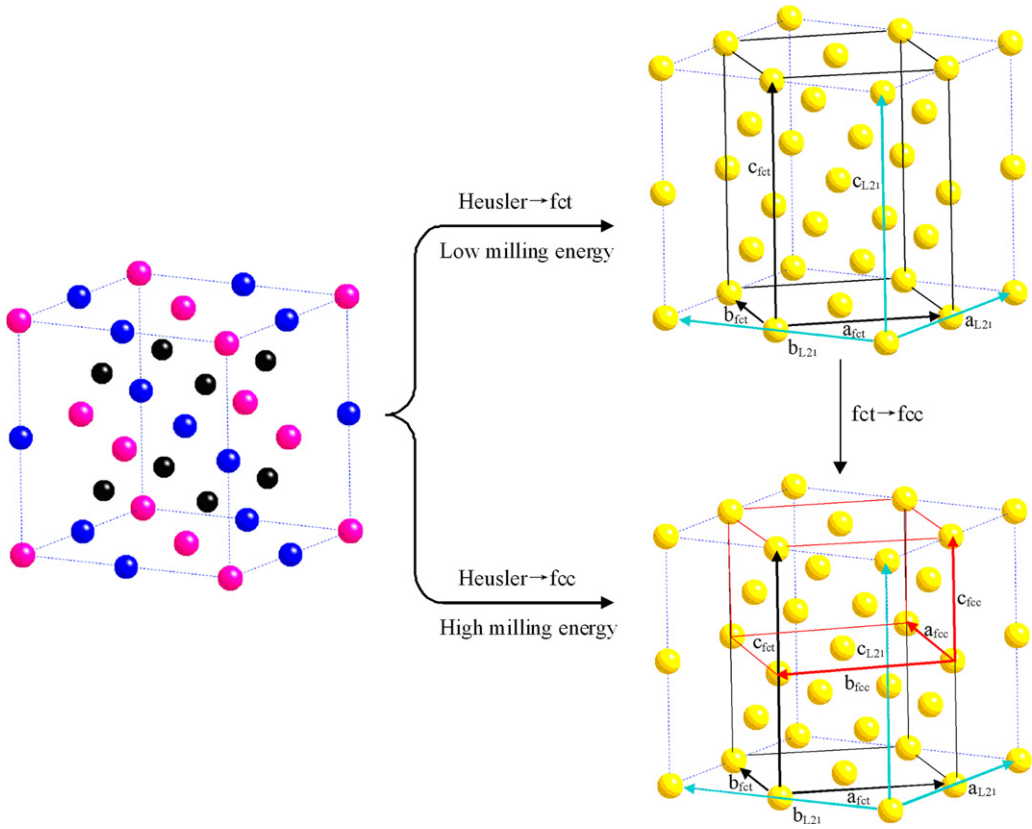

Fig. 3. A schematic illustration for the Heusler ($L2_1$)→fct and Heusler ($L2_1$)→fcc structural transition of Ni–Mn–Ga alloy in the low and high energy milling process, respectively. Left figure: Heusler structure with Ni, Mn and Ga atoms at respective sites colored in black, pink and blue, respectively. Right two figures: disordered structure with mixed Ni, Mn and Ga atoms at all sites colored in yellow. (For interpretation of the references to color in this figure legend, the reader is referred to the web version of the article.)

of $L2_1$ have also been indicated in the disordered structure. In the model, the volume relation between the fct structure and the original Heusler structure is $v_{fct} = (1/2)v_{L2_1}$. In the experimental result, $a_{fct} = 0.39060$ nm $< (\sqrt{2}/2)a_{L2_1} = 0.41287$ nm and $c_{fct} = 0.65479$ nm $> c_{L2_1} = 0.58388$ nm. By calculating, the volume of the disordered fct phase is $v_{fct} = (a_{fct})^2 \times c_{fct} = (0.3906)^2 \times 0.65479 = 0.0999\,nm^3$ and the volume of the Heusler phase is $v_{L2_1} = (a_{L2_1})^3 = 0.58388^3 = 0.199\,nm^3$, so the result is $v_{fct} \approx (1/2)v_{L2_1}$, which is consistent with the value calculated in the model. On the basis of the above calculation and the principle that the volume keeps constant before and after deformation of the crystal lattice, it is considered that the ball milling with low milling energy introduce atomic disorder and small lattice distortion to the Ni–Mn–Ga alloy, which makes small contraction of a_{L2_1} and b_{L2_1} and elongation of c_{L2_1} to result in the formation of the disordered fct structure phase. According to the indication in the model, the approximate lattice correspondence between the fct phase and the Heusler phase should be $\vec{a}_{fct} = (1/2)a_{L2_1}[1\,\bar{1}\,0]$, $\vec{b}_{fct} = (1/2)a_{L2_1}[1\,1\,0]$ and $\vec{c}_{fct} = \vec{c}_{L2_1}$, which is consistent with the previous report [23].

For the process with high milling energy (vibration ball milling), the analysis is similar to the above description, the fcc structure as circled by red line in the lower part of Fig. 3 is assumed to appear in the disordered structure. In this model, $v_{fcc} = (1/2)v_{fct}$. According to the experimental result, $a_{fcc} = 0.36646$ nm $< a_{fct} = 0.39060$ nm and $c_{fcc} = 0.36646$ nm $> (1/2)c_{fct} = 0.32740$ nm. After calculation, $v_{fcc} = (a_{fcc})^3 = 0.36646^3 = 0.0492\,nm^3$, so $v_{fcc} \approx (1/2)v_{fct}$, which is also consistent with the result attained in the model. By comparison of the lattice parameters for the disordered fct and fcc structures between the above model and experimental results, it is derived that the fcc phase should result from a further lattice deformation of the fct phase. Hereby, the fcc structure is achieved by suffering a bigger lattice distortion than the fct structure during ball milling. So it can be considered that the ball milling with high milling energy introduce atomic disorder and large lattice distortion (compared with the small lattice distortion in fct structure caused by low milling energy) into the Ni–Mn–Ga alloy, which makes a big contraction of a_{L2_1} and b_{L2_1} and elongation of c_{L2_1} to lead to the formation of the disordered fcc structure phase. As shown in the figure, the approximate lattice correspondence between the fcc phase and the Heusler phase should be $\vec{a}_{fcc} = (1/2)a_{L2_1}[1\,1\,0]$, $\vec{b}_{fcc} = (1/2)a_{L2_1}[\bar{1}\,1\,0]$ and $\vec{c}_{fcc} = (1/2)\vec{c}_{L2_1}$.

Based on the above analysis, the disordered fct and disordered fcc phases are expected to form from the Heusler phase after the ball milling with low and high milling energy, respectively. It is also noted that the structural transition from disordered fct to disordered fcc is possible to occur in the ball milling process when a suitable milling energy is performed, as shown in the right part of Fig. 3.

Fig. 4(a) shows DSC curves at different heating rates for the Ni–Mn–Ga powder milled for 4 h. An exothermic event was detected at ~320 °C with the heating rate of 10 °C/min. No exothermic events are detected in the subsequent cooling and second heating, which indicates this exothermic process is irreversible. It is different from the result observed in the Ni–Mn–Ga powders milled by planetary ball milling [22], in which two exothermic peaks are detected at 305 °C and 410 °C during heating. These two exothermic peaks are attributed to the structural transition from disordered fct to disordered bcc and from disordered bcc to Heusler structure, respectively. According to the XRD results in Fig. 5 (it will be described in the following paragraph), the exothermic event should correspond to the structural transition

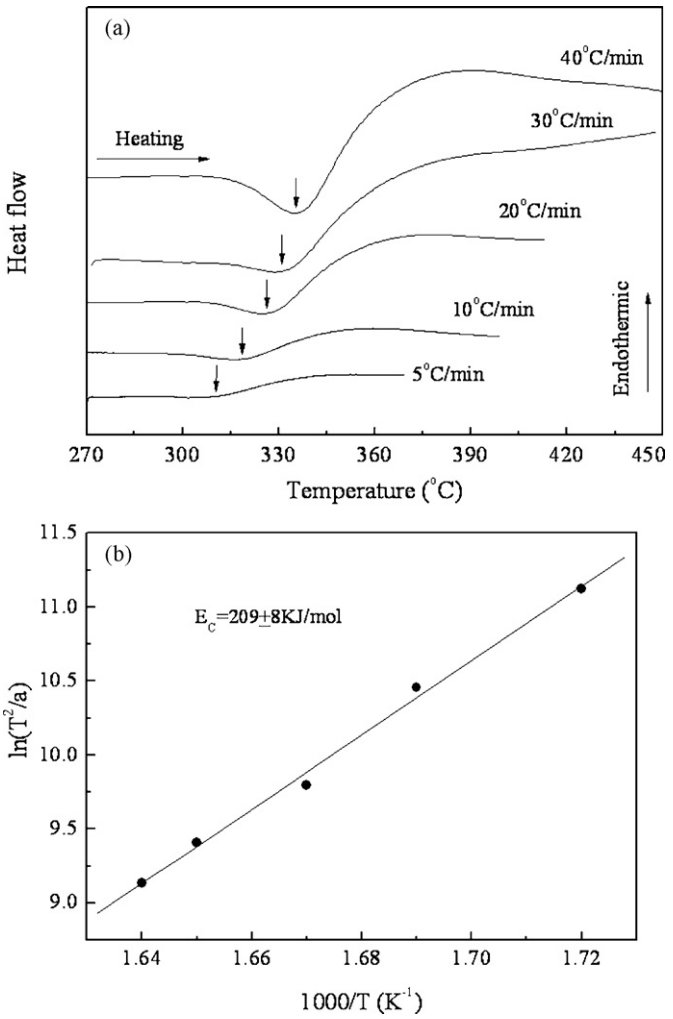

Fig. 4. (a) DSC curves of 4 h milled Ni–Mn–Ga powder upon heating at different heating rates and (b) plot of $\ln(T^2/a)$ against $1/T$.

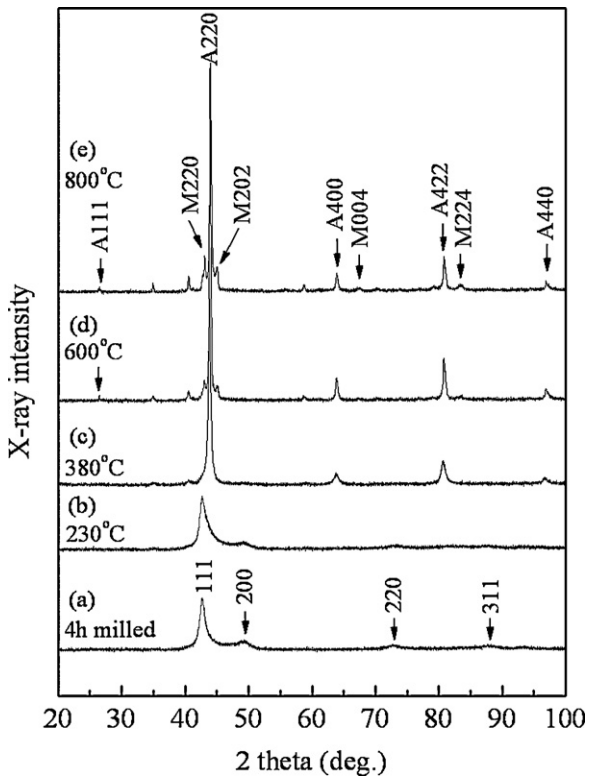

Fig. 5. Room temperature XRD patterns for the 4 h milled Ni–Mn–Ga powder (a) and the Ni–Mn–Ga powders annealed at 230 °C (b), 380 °C (c), 600 °C (d) and 800 °C (e).

from disordered fcc to disordered bcc. However, the exothermic event associated with structural transition from disordered bcc to Heusler as described in Ref. [22] is not detected on heating up to 500 °C for the present powder. It is noticed that the transition temperature of disordered fcc → disordered bcc (320 °C) is higher than that of disordered fct → disordered bcc (305 °C). With increasing heating rate, the exothermic peak for the structural transition of disordered fcc → disordered bcc shifts towards higher temperatures. The peak shift and the heating rate can be well correlated to each other by Kissinger's equation [26]: $\ln(T^2/a) = E_c/RT + C$, where a is the heating rate (K/min), E_c is the activation energy, R is the gas constant (8.314 J K^{-1} mol^{-1}), and C is a constant. This equation defines a linear relationship between $\ln(T^2/a)$ and $1/T$, as shown in Fig. 4(b). The activation energy for this transition determined from the slope of the line is 209 ± 8 kJ/mol. It is lower than the activation energy for the crystallization of $Ni_{51.45}Mn_{25.3}Ga_{23.25}$ thin film prepared by r.f. magnetron sputtering [27], which may be caused by that more energy for crystallization (lattice recovery and ordering of atoms) is needed than that for the structural transition of disordered fcc → disordered bcc (lattice recovery).

Fig. 5 shows the room temperature XRD patterns of the 4 h milled Ni–Mn–Ga powder and the annealed Ni–Mn–Ga powders. The pattern of the 4 h milled Ni–Mn–Ga powder sample (Fig. 5(a)) is same with the result shown in the Fig. 2(f). It can be seen that the diffraction peaks belonging to the milled Ni–Mn–Ga powder sample slightly become weaker after 230 °C annealing, as shown in Fig. 5(b). After 380 °C annealing, all the peaks corresponding to the milled Ni–Mn–Ga powder disappeared and four other diffraction peaks centered at $2\theta = 43.9°$, 63.8°, 80.7° and 96.7° appeared. These new peaks can be indexed as a disordered bcc structure phase [22]. The exothermic event centered at 320 °C in the DSC curve (Fig. 4(a)) just falls between 230 °C and 380 °C. Therefore, the exothermic event should correspond to the structural transition process from disordered fcc to disordered bcc. This process should be an elimination of the lattice distortion caused by ball milling based on the analysis in Fig. 3, when the bcc unit cell is the smallest unit in the disordered structure phase. With annealing temperature increasing to 600 °C, the (1 1 1) superlattice peak of the Heusler austenite appears at $2\theta = 26.5°$, indicating the formation of Heusler phase with high atomic order. This shows the occurrence of the atomic ordering process with annealing temperature increasing to 600 °C (disordered bcc → Heusler), though the exothermic event associated with this process is not detected in the DSC curve up heating to 500 °C (Fig. 4(a)). The Ni–Mn–Ga powder annealed at 600 °C can be indexed to consist of the Heusler austenite phase and 5 M tetragonal martensite phase. However, the austenite predominantly exists in the Ni–Mn–Ga powder and the content of the martensite is few, according to comparison of the relative intensity of diffraction peaks, which is different from the result of bulk Ni–Mn–Ga alloy shown in the Fig. 2(a). The Ni–Mn–Ga powder annealed at 800 °C shows a similar diffraction pattern with the sample annealed at 600 °C, but with a little increase of the relative intensity of diffraction peaks for the martensite phase.

Fig. 6(a) shows the DSC curves of the bulk Ni–Mn–Ga alloy and the Ni–Mn–Ga powder annealed at 800 °C. The as-milled Ni–Mn–Ga powder and powders annealed at 230 °C, 380 °C and 600 °C do not show martensitic transformation, so their DSC curves are not shown in the figure. It can be seen that the bulk Ni–Mn–Ga alloy shows a strong one-step martensitic transformation behavior,

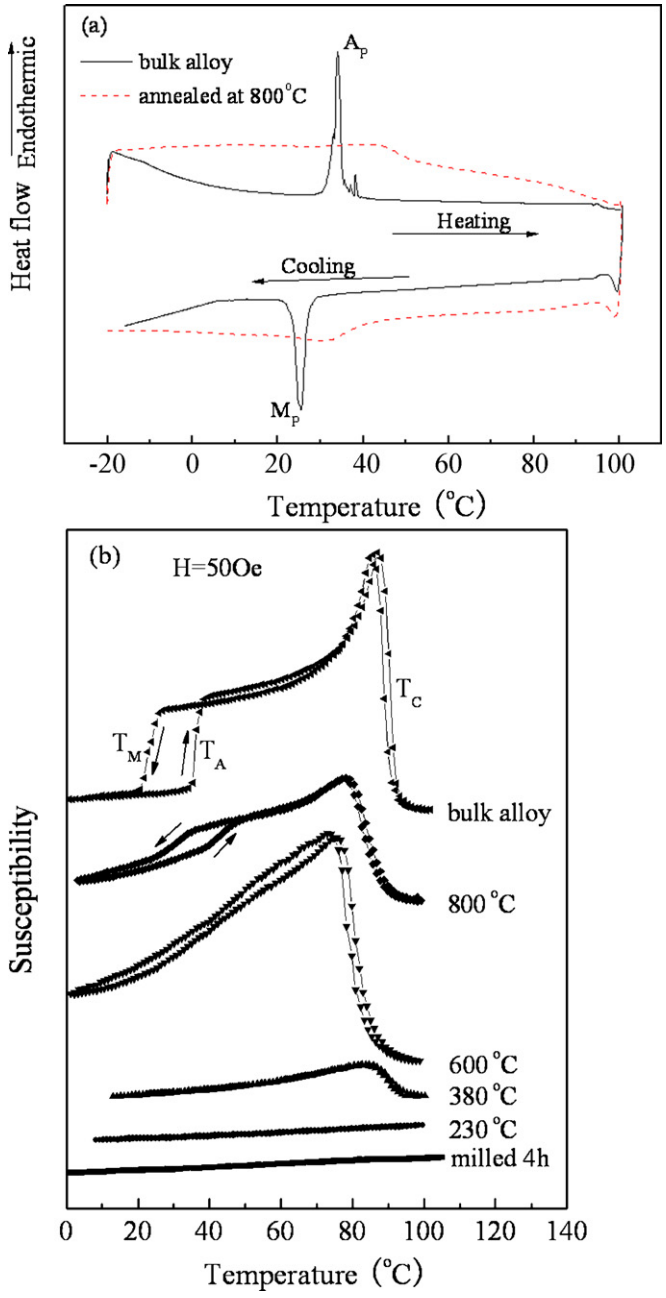

Fig. 6. (a) DSC curves of the bulk Ni–Mn–Ga alloy and 800 °C annealed Ni–Mn–Ga powder with heating rate of 10 °C/min and (b) the temperature dependence of low-field ac magnetic susceptibility curves for bulk Ni–Mn–Ga alloy, 4 h milled Ni–Mn–Ga powder and the Ni–Mn–Ga powders annealed at 230 °C, 380 °C, 600 °C and 800 °C. The field was 50 Oe.

while 800 °C annealed Ni–Mn–Ga powder sample exhibits a very weak one-step martensitic transformation behavior in the similar temperature range. The 800 °C annealed Ni–Mn–Ga powder is cooled to −200 °C and heated to room temperature, no other transformation peaks are observed in the DSC curve. The M_p and A_p marked in the curve indicate the peak temperatures of the martensitic and austenitic transformation, respectively. It is seen that the annealed Ni–Mn–Ga powder show a little higher transformation temperature (~5 °C) than the bulk Ni–Mn–Ga alloy. The latent heat of martensitic transformation for the annealed Ni–Mn–Ga powder is quite lower than that for the bulk Ni–Mn–Ga alloy, indicating the volume fraction taking part in the transformation is smaller.

Fig. 6(b) shows the ac susceptibilities of the bulk Ni–Mn–Ga alloy, as-milled Ni–Mn–Ga powder, and the annealed Ni–Mn–Ga powders with the variation of temperature in a field of 50 Oe. For the bulk Ni–Mn–Ga alloy, upon cooling, there is a sudden increase of the susceptibility at ~90 °C, which corresponds to the Curie transition of the austenite. When the temperature is further lowered down to ~24 °C, an abrupt decrease of susceptibility occurs, which indicates the occurrence of austenite → martensite transformation. Upon heating, the increase of susceptibility at ~36 °C stands for the martensite → austenite transformation. T_M, T_A and T_C marked on the maximum slope of the curves represent the transition temperatures for the austenite → martensite, martensite → austenite and Curie transition, respectively. For the milled Ni–Mn–Ga sample and annealed Ni–Mn–Ga samples, it can be seen that the 4 h milled Ni–Mn–Ga powder does not show martensitic transformation, and annealed at 230 °C, 380 °C and 600 °C can also not recover the martensitic transformation, but annealed at 800 °C make the martensitic transformation appear. The T_M and T_A of the 800 °C annealed Ni–Mn–Ga powders are little higher (~6 °C) than that of the bulk Ni–Mn–Ga alloy. The martensitic transformation behavior of the 800 °C annealed Ni–Mn–Ga powder is weaker than that of the bulk Ni–Mn–Ga alloy. These results obtained in the ac susceptibility measurements are consistent with that measured in the above DSC curves. It is also noted that in the Fig. 6(b), though the martensitic transformation is not recovered in the low temperatures (230 °C, 380 °C and 600 °C) annealed samples, the Curie transition retrieve gradually with the increase of the annealing temperature. The occurrence of the Curie transition before the occurrence of the martensitic transformation during annealing is attributed to the fact that the requirement of atomic ordering level for the second-order Curie transition is lower than that for the first-order martensitic transformation [23].

For the Ni–Mn–Ga powder annealed at 600 °C, the invisibility of martensitic transformation in the DSC and ac susceptibility measurements cannot be understood at present, because the powder is composed of the austenite and martenite phase at room temperature (Fig. 5(d)). For the Ni–Mn–Ga powder annealed at 800 °C, the low volume of martensitic transformation indicates that a large amount of Heusler austenite phases in the powder may not transform to the martensite phase upon cooling process. It has been reported that when the grain size is smaller than a critical size in the Ni–Ti bulk alloy (<60 nm) [28] and Ni–Mn–Sn film with thickness of ~1 μm (<10.8 nm) [29], the martensitic transformation is fully suppressed. The grain size of the present Ni–Mn–Ga alloy can be reduced after high energy ball milling and the growth of grain size during the post-annealing process is also possibly constrained in the thickness direction due to the small thickness (~1 μm) of the resulted particles shown in Fig. 1(a). Therefore, the grain refinement of the austenite phase possibly results in the disappearance of martensitic transformation of the annealed Ni–Mn–Ga particles.

4. Conclusions

The Ni–Mn–Ga powder particles in flaky shape with disordered fcc structure are prepared by vibration ball milling. The atomic disorder and large lattice distortion introduced in the Ni–Mn–Ga alloy during the ball milling process makes the alloy transform from Heusler phase to the disordered fcc phase. Upon heating, the disordered fcc phase transforms to the disordered bcc phase at ~320 °C due to the elimination of the lattice distortions. The activation energy for this transition process is 209 ± 8 kJ/mol. The Ni–Mn–Ga powder annealed at 800 °C shows a weak martensitic transformation behavior. The suppression of the partial martensitic transformation in the annealed Ni–Mn–Ga powders may be related to the grain refinement of the austenite phase in the powder

particles. For considering the practical application, the martensitic transformation property of the present Ni–Mn–Ga powders is needed to be improved further.

Acknowledgement

The work was supported by the Fundamental Research Funds for the Central Universities (HEUCF101013).

References

[1] K. Ullakko, J.K. Huang, C. Kantner, R.C. O'Handley, V.V. Kokorin, Appl. Phys. Lett. 69 (1996) 1966–1968.
[2] K. Ullakko, J.K. Huang, V.V. Kokorin, R.C. O'Handley, Scr. Mater. 36 (1997) 1133–1138.
[3] S.J. Murray, M. Marioni, S.M. Allen, R.C. O'Handley, Appl. Phys. Lett. 77 (2000) 886–888.
[4] A. Sozinov, A.A. Likhachev, N. Lanska, K. Ullakko, Appl. Phys. Lett. 80 (2002) 1746–1748.
[5] G. Girard, S. Béchu, N. Caillault, L. Carbone, L. Ortega, D. Fruchart, J. Alloys Compd. 465 (2008) 35–40.
[6] H.B. Wang, C. Liu, Y.C. Lei, W. Cai, J. Alloys Compd. 465 (2008) 458–461.
[7] O. Heczko, M. Thomas, R. Niemann, L. Schultz, S. Fähler, Appl. Phys. Lett. 94 (2009) 152513.
[8] W. Cai, C. Liu, H.B. Wang, Z.Y. Gao, J. Alloys Compd. 468 (2009) 200–202.
[9] J. Tillier, D. Bourgault, B. Barbara, S. Pairis, L. Porcar, P. Chometon, D. Dufeu, N. Caillault, L. Carbone, J. Alloys Compd. 489 (2010) 509–514.
[10] J.M. Wang, C.B. Jiang, R. Techapiesancharoenkij, D. Bono, S.M. Allen, R.C. O'Handley, J. Appl. Phys. 106 (2009) 023923.
[11] N.V. Rama Rao, R. Gopalan, V. Chandrasekaran, K.G. Suresh, J. Alloys Compd. 478 (2009) 59–62.
[12] S.C. Ma, Q.Q. Cao, H.C. Xuan, C.L. Zhang, L.J. Shen, D.H. Wang, Y.W. Du, J. Alloys Compd. 509 (2011) 1111–1114.
[13] H. Hosoda, S. Takeuchi, T. Inamura, K. Wakashima, Sci. Technol. Adv. Mater. 5 (2004) 503–509.
[14] J. Feuchtwanger, M.L. Richard, Y.J. Tang, A.E. Berkowitz, R.C. O'Handley, S.M. Allen, J. Appl. Phys. 97 (2005) 10M319.
[15] N. Scheerbaum, D. Hinz, O. Gutfleisch, K.-H. Muüller, L. Schultz, Acta Mater. 55 (2007) 2707–2713.
[16] N. Scheerbaum, D. Hinz, O. Gutfleisch, W. Skrotzki, L. Schultz, J. Appl. Phys. 101 (2007) 09C501.
[17] M. Lahelin, I. Aaltio, O. Heczko, O. Söerberg, Y. Ge, B. Lögren, S.-P. Hannula, J. Seppälä, Composites A 40 (2009) 125–129.
[18] J. Liu, N. Scheerbaum, S. Weiß, O. Gutfleisch, Appl. Phys. Lett. 95 (2009) 152503.
[19] B. Tian, F. Chen, Y.X. Tong, L. Li, Y.F. Zheng, Mater. Lett. 63 (2009) 1729–1732.
[20] B. Tian, F. Chen, Y.X. Tong, L. Li, Y.F. Zheng, Y. Liu, J. Alloys Compd. 505 (2010) 680–684.
[21] V.C. Solomon, J. Hong, Y.J. Tang, A.E. Berkowitz, D.J. Smith, Scr. Mater. 56 (2007) 593–596.
[22] B. Tian, F. Chen, Y. Liu, Y.F. Zheng, Mater. Lett. 62 (2008) 2851–2854.
[23] B. Tian, F. Chen, Y. Liu, Y.F. Zheng, Intermetallics 16 (2008) 1279–1284.
[24] F. Chen, B. Tian, L. Li, Y.F. Zheng, Trans. Nonferr. Met. Soc. China 17 (2007) s614–s617.
[25] Y.D. Wang, Y. Ren, Z.H. Nie, D.M. Liu, L. Zuo, H. Choo, H. Li, P.K. Liaw, J.Q. Yan, R.J. McQueeney, J.W. Richardson, A. Huq, J. Appl. Phys. 101 (2007) 063530.
[26] H.E. Kissinger, Anal. Chem. 29 (1957) 1702–1706.
[27] S.K. Wu, K.H. Tseng, J.Y. Wang, Thin Solid Films 408 (2002) 316–320.
[28] T. Waitz, V. Kazykhanov, H.P. Karnthaler, Acta Mater. 52 (2004) 137–147.
[29] R. Vishnoi, D. Kaur, Surf. Coat. Technol. 204 (2010) 3773–3782.